Supplement of Atmos. Meas. Tech., 19, 1365–1383, 2026
https://doi.org/10.5194/amt-19-1365-2026-supplement

Atmospheric Measurement Techniques
Open Access
EGU

Supplement of

The role of size in the multiple scattering correction *C* for dual-spot aethalometer: a field and laboratory investigation

Laura Renzi et al.

Correspondence to: Laura Renzi (l.renzi@isac.cnr.it)

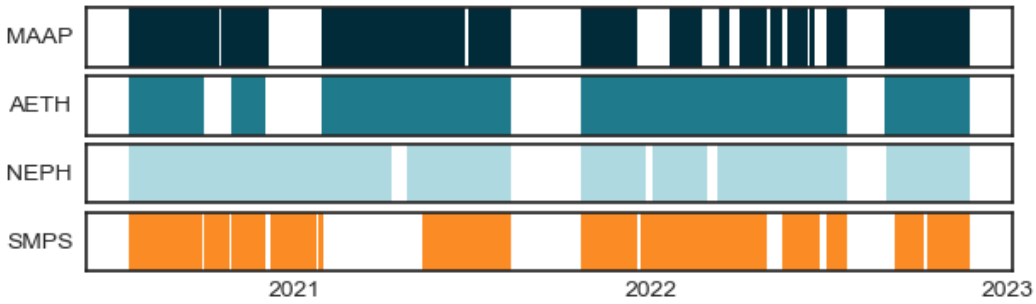

Figure S1: Instrument availability at CMN for MAAP, Nephelometer, Aethalometer and SMPS.

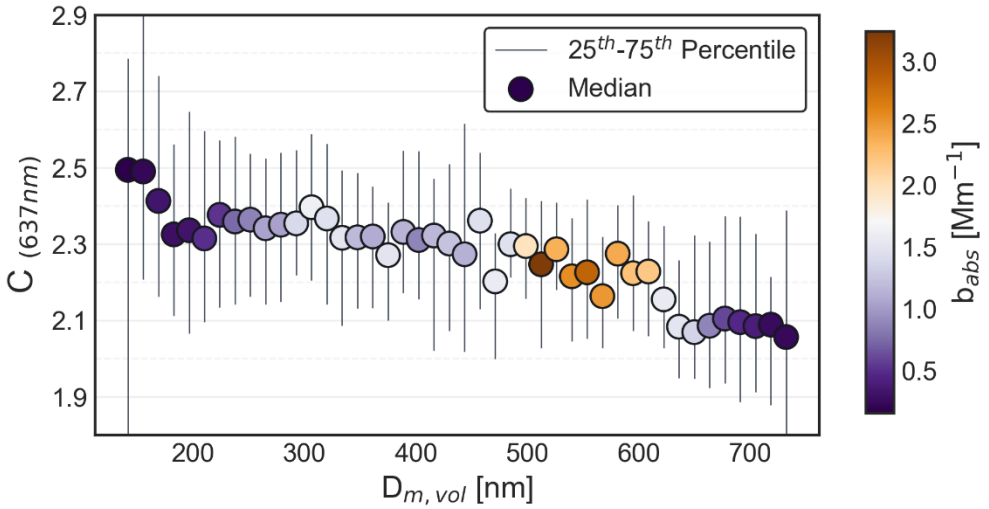

Figure S2: Cross-sensitivity of the C-size dependence on absorption coefficient measured by the MAAP. The color of the dots follows the variability of the median absorption coefficient in each size bin.

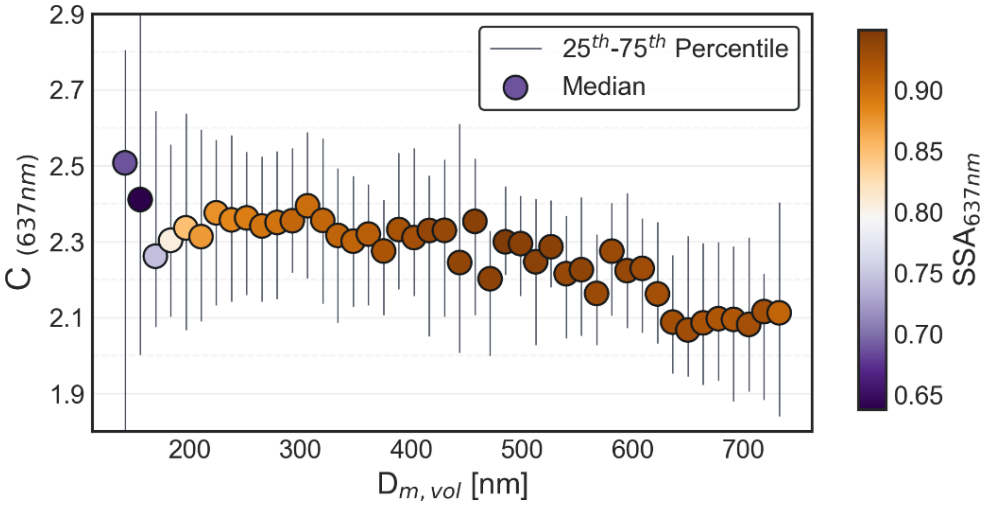

Figure S3: Cross-sensitivity of the C-size dependence on the SSA. The color of the dots follows the variability of the median SSA in each size bin.

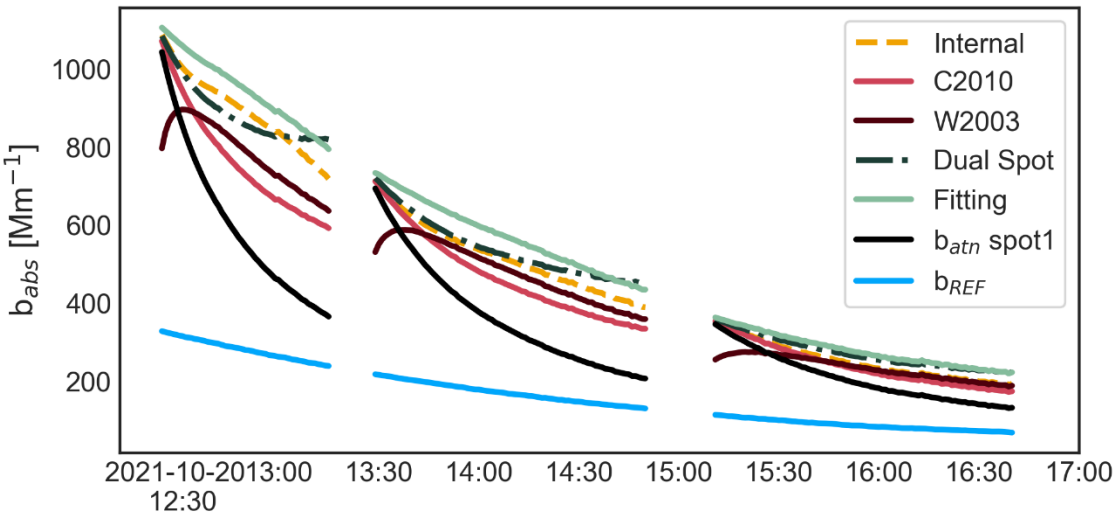

Figure S4: Variation of b_{atn} and b_{abs} at one-minute resolution during a representative chamber experiment. The periods of interruption in the series correspond to the aethalometer filter changes. The lines represent the reference measurement, the attenuation coefficient uncorrected for loading measured in spot 1 of the aethalometer at 660 nm, the loading-corrected attenuation coefficient using the C2010, W2003, Internal method, Dual Spot and Fitting methods, respectively.

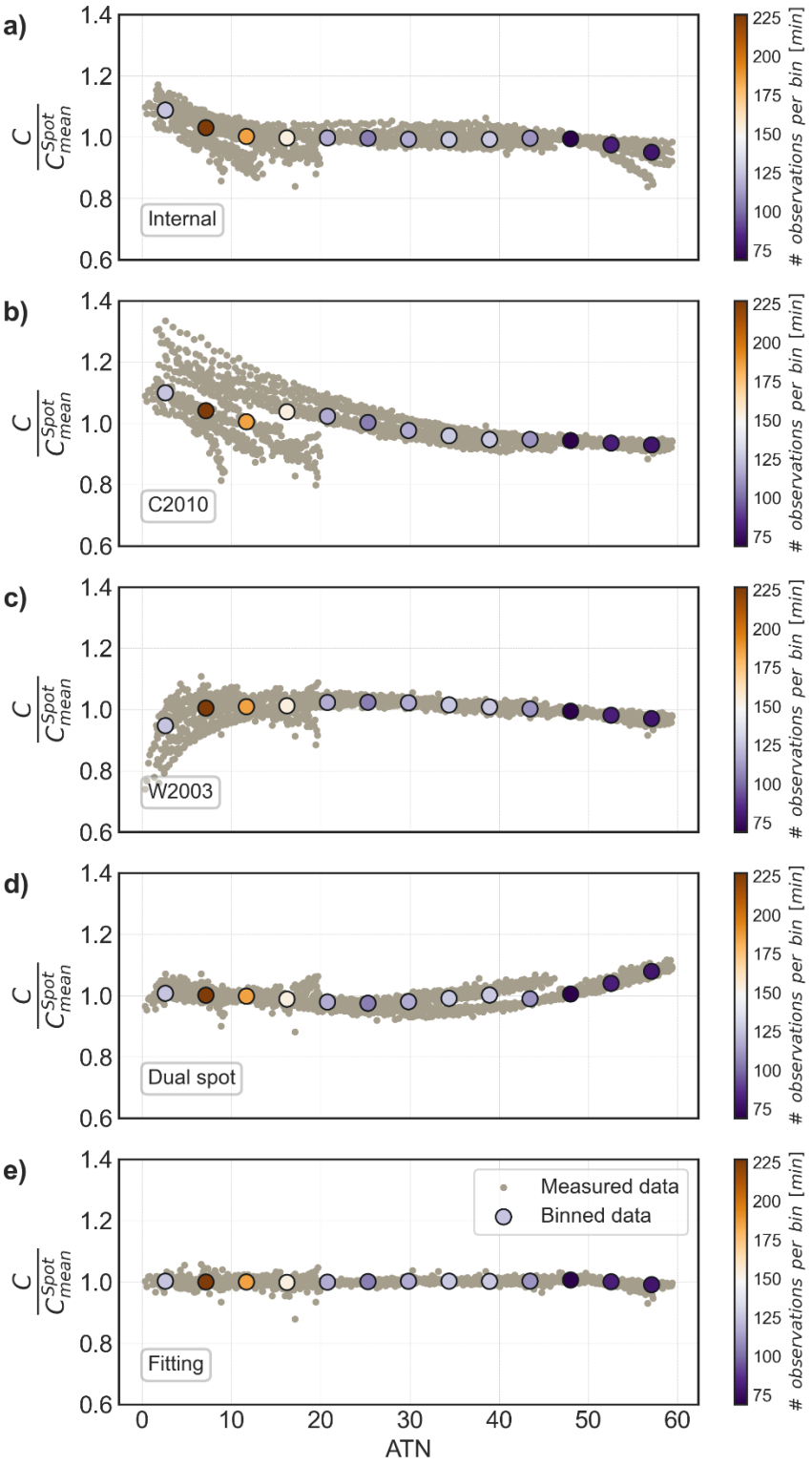

Figure S5: Variability of C values normalized for their average in each filter spot with attenuation at 660 nm. The grey points represent the one-minute resolution C values, while the colored points indicate the median values for each attenuation bin. The color intensity corresponds to the number of data points within each bin, providing a clear visualization of the data distribution. Data correspond to all CS1-CS5 experiments.

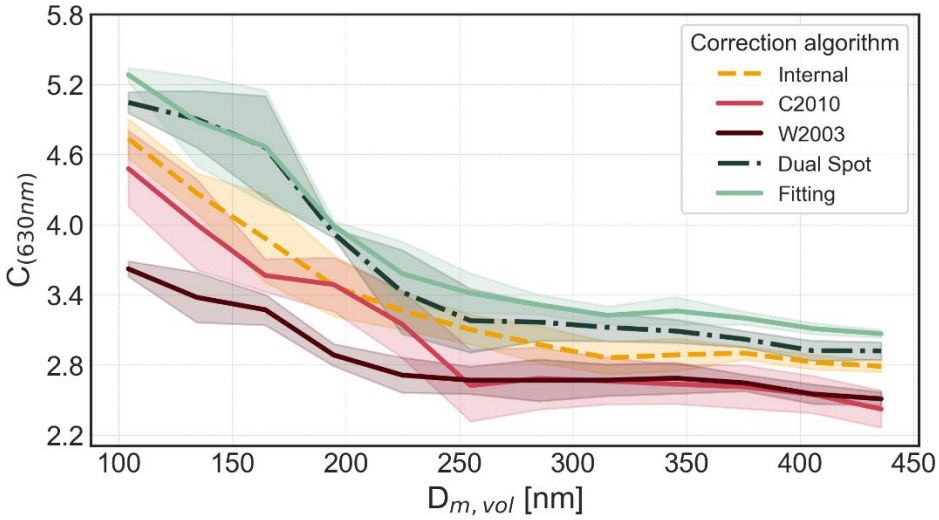

Figure S6: C dependence on particle size in laboratory studies. One-minute resolution C values are binned on the volume mean diameter ($D_{m,vol}$). The line represents the mean values in each bin the coloured area the mean ± the standard deviation. One line is displayed for the C values derived from $b_{atn,LC}$ loading corrected using different methods (Internal, C2010, W2003, Dual Spot and the 'Fitting' method).

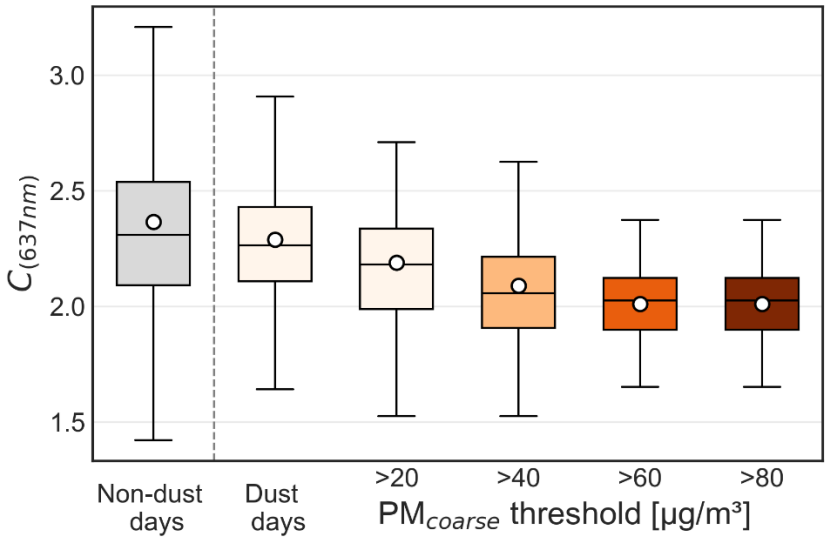

Figure S7: Boxplot comparing C values statistics during non-dust days and dust days of increasing intensity represented by increasing threshold in the PM coarse fraction measured by an OPC during transport events. The identification of dust events at CMN is done according to the method detailed in Vogel et al., 2025 as well as the quantification of PM coarse.

Table S1. Physico-chemical properties of the Cast Soot (CS) aerosols for the five combustion conditions considered in this study (CS1 to CS5) corresponding to the first five predefined miniCAST operation points (OP1 to OP5) (Heuser et al., 2025).

Cast Soot Type	**miniCAST flowrates fuel/mix. N_2/ox. Air [L min^{-1}]**	**Combustion condition**	**Global equivalence ratio (φ)**	**CMD_{60min} (D_m) [nm]**	**Mobility exponent (D_{fm})**	**Fractal dimension (D_f)**	**Avg. Primary particle diameter (D_{pp}) [nm]**	**EC/TC**
CS1 (OP1)	0.03/0/0.75	Fuel lean	0.91	145 ± 12	2.11 ± 0.04	1.91 ± 0.22	9.8 ± 1.9	0.79 ± 0.11
CS2 (OP2)	0.025/0/0.60	Fuel lean	0.95	138 ± 1	2.10 ± 0.04	2.04 ± 0.24	7.2 ± 2.5	0.73 ± 0.08
CS3 (OP3)	0.025/0.01/0.60	Fuel lean	0.95	122 ± 9	2.10 ± 0.04	1.79 ± 0.20	15.4 ± 1.9	0.67 ± 0.09
CS4 (OP4)	0.023/0.02/0.60	Fuel lean	0.88	103 ± 17	2.20 ± 0.04	1.83 ± 0.22	10.0± 1.7	0.53 ± 0.13
CS5 (OP5)	0.023/0.02/0.45	Fuel rich	1.20	79 ± 2	2.25 ± 0.04	–	–	0.00 ± 0.22

Table S2. Summary of experimental conditions investigated during simulation chamber experiments at the CESAM chamber. The acronym CS stands for Cast Soot and CS1 to CS5 refers to particles generated under the five setting points of the miniCAST summarized in Table S1. The concentration of the CS at the peak of the injection as derived from SMPS and CPMA measurements (see Section S1). The date and time of start/end refer to the time periods within each experiment used for absorption measurements. The averages considered for C calculation correspond then to each aethalometer filter spot change inside these periods. The time since CS injection in CESAM to which the start of the experiment correspond is indicated.

Experiment	CS concentration at peak (µg m^{-3})	Date time start	Date time end	Time from injection (hh:mm)
CS1	61 ± 6	2021-10-19 12:31	2021-10-19 17:00	01:21-05:50
CS1	157 ± 19*	2022-12-12 11:35	2022-12-12 11:56	01:14-01:35
CS1	166 ± 20*	2022-12-14 10:25	2022-12-14 11:41	00:24-01:40
CS1	167 ± 21*	2022-12-15 11:50	2022-12-15 12:31	00:21-01:02
CS1	171 ± 21*	2022-12-16 11:57	2022-12-16 12:47	00:46-01:36
CS2	95 ± 8	2021-10-20 12:24	2021-10-20 16:41	00:46-05:03
CS3	89 ± 8	2021-10-26 11:49	2021-10-26 15:45	00:46-04:42
CS3	151 ± 20*	2022-12-06 09:40	2022-12-06 11:28	00:20-02:08
CS3	219 ± 29*	2022-12-07 11:35	2022-12-07 12:19	01:07-01:51
CS4	44 ± 4	2021-10-22 12:05	2021-10-22 16:59	01:15-06:09
CS5	46 ± 4	2021-05-28 11:54	2021-05-28 13:08	01:29-03:23
CS5	65 ± 7	2021-10-21 12:25	2021-10-21 14:12	00:11-01:58
CS5	127 ± 23*	2022-12-08 11:37	2022-12-08 13:15	00:05-01:43
CS5	121 ± 22*	2022-12-09 10:13	2022-12-09 11:50	00:11-01:48

* average masses calculated using the two CAPS signals and the MECs provided in Heuser et al., 2025 for the CSs

Table S3. Average C values, and their standard deviations, determined from one-minute resolution attenuation coefficient and absorption coefficient values, corrected for the loading effect using different methods; AE33 internal correction, W2003, C2010, Dual Spot, and an experiment fitting specifically obtained for this study.

Method	Internal correction	W2003	C2010	Dual Spot	Fitting
Mean (SD)	3.16 (0.50)	2.77 (0.3)	2.88 (0.56)	3.40 (0.64)	3.54 (0.6)

Table S4. Mean k values derived applying the Dual Spot method to all filter spot for each CS type.

	CS1	CS2	CS3	CS4	CS5
k mean	0.0101	0.0097	0.0112	0.0125	0.0224

S1. Loading correction schemes applied to chamber experiments

For chamber experiments the internal AE33 correction can provide uncertain results due to high soot concentration, frequent filter changes (tens of minutes-few hours), operating conditions highly variable between experiments, and experiment durations relatively short. As illustrated in Fig. S4 the time variability of the $b_{atn,LC}$ does not follow the same decreasing trend over time as the reference measurement. However, it shows a steeper decline before and after the filter change, with a more rapid decrease in these points, making the trend appear more abrupt and also discontinuous around the filter transition. In this case the AE33 data were re-corrected for loading effect. To do this, the AE33 was treated like a single-spot aethalometer. The b_{atn} for the first spot (the one with higher flow rate) at one-minute resolution are considered. Three approaches are used to estimate three sets of $b_{atn,LC}$:

- the W2003 correction scheme: this approach assumes that the real absorption is measured at 10% of ATN and that the loading effect, represented by the loading correction R_{W2003}, results in a logarithmic dependence of b_{atn} vs ATN through a factor f(λ) as follows:

$$b_{atn,LC,W2033}(\lambda) = \frac{b_{atn}(\lambda)}{R_{W2003}(\lambda)} = \frac{b_{atn}(\lambda)}{\left[\left(\frac{1}{f(\lambda)} - 1\right) \cdot \frac{lnATN(\lambda) - \ln(10\%)}{\ln(50\%) - \ln(10\%)} + 1\right]} \quad (S1)$$

The f(λ) function can be expressed as a function of the particles SSA as $f(\lambda) = a(1 - SSA) + 1$ with a equal to 0.87 (450 nm) and 0.85 (660 nm) in W2003.

- the C2010 correction scheme: this formulation assumes no loading effect at 0% ATN and a linear relationship between b_{atn} and ATN. The $b_{atn,LC,C2010}(\lambda)$ according to C2010 is obtained as:

$$b_{atn,LC,C2010}(\lambda) = \frac{b_{atn}(\lambda)}{R_{C2010}(\lambda)} = \frac{b_{atn}(\lambda)}{\left(\frac{1}{f(\lambda)} - 1\right) \cdot \frac{ATN(\lambda)}{50\%} + 1} \quad (S2)$$

where R_{C2010} is the loading correction expressed as in W2003 with a = 0.74.

- the Dual Spot method defined in Drinovec et al., (2015; equations 3 and 4) applied, using a constant compensation parameter, to batn/bREF instead of BC as follows:

$$\frac{b_{atn}}{b_{REF}} = \left(\frac{b_{atn}}{b_{REF}}\right)_0 (1 + RS \cdot ATN), \quad (S3)$$

$$RS = \left(\frac{b_{REF}}{b_{atn}}\right)_0 \cdot \frac{d\left(\frac{b_{atn}}{b_{REF}}\right)}{dATN}. \quad (S4)$$

The RS and $\left(\frac{b_{REF}}{b_{atn}}\right)_0$ were obtained through a linear fit applied to each filter spot and used to obtain the k values for correcting b_{atn} according to Drinovec et al., (2015; equation 7). Table S4 summarizes the averaged k values for each CS type.

- the last approach used is developed specifically for this study, hereafter referred as 'fitting'. As a matter of fact, both W2003 and C2010 correction approaches results in $b_{atn,LC}$ whose temporal variation does not follow the evolution of the mass concentration in the chamber (Figure S4). This correction is based on few assumptions that we considered valid for the studied experiments. In particular, the temporal variability of the loading-corrected

attenuation coefficient measured by the aethalometer must match that of the reference technique. Therefore, C is considered approximately constant within a filter spot. This assumption is an acceptable approximation in the experiments considered, where the properties of the particles change slowly during each experiment, as reported by Heuser et al. (2025). The attenuation value at which the loading effect is negligible is 0. The best function representing the dependence of b_{atn}/b_{ref} on ATN in these assumption was a second degree polynomial equation. The $b_{atn,LC,fitting}(\lambda)$ according to this fitting method is thus obtained as:

$$b_{atn,LC,fitting}(\lambda) = \frac{b_{atn}(\lambda) \cdot c_1}{a_1 \cdot ATN(\lambda)^2 + b_1 \cdot ATN(\lambda) + c_1} \quad (S3)$$

where the parameters a_1, b_1, c_1 were obtained by fitting the ratio b_{atn}/b_{ref} on ATN, and were derived separately for any filter spot. The primary advantage of applying this method is that it completely flattens the dependence of the loading-corrected attenuation coefficient on attenuation, whereas other methods retain this dependence (Figure S5). Additionally, it improves the continuity of the measured values between the end of one filter spot and the beginning of the next, eliminating any jumps in the values (Figure S4).

S2. Dependence of C on the attenuation and loading correction scheme from chamber experiments

The loading effect correction scheme is critical especially under high concentrations of absorbing species and by consequence it can affect the retrieved C. Particularly, biases can arise immediately before and after filter changes, despite the internal loading correction applied (Cuesta-Mosquera et al., 2021). To investigate this aspect, the potential residual dependence of C on attenuation is analyzed taking advantage of the measurements in controlled chamber conditions. Indeed, as shown by Heuser et al. (2025), the properties of the CS1-CS5 (size, SSA, MAC) varied little during a filter spot cycle, therefore for each filter spot interval C should theoretically be independent of attenuation if the loading effect has been properly corrected. The analysis of this dependence was performed using C values at 630 nm, derived with a time resolution of one minute from $b_{atn,LC,Internal}$ (630 nm) normalized to the mean C value for each spot. The results are illustrated in Fig. S5 reporting the normalized C as a function of the attenuation at 660 nm for all data acquired during chamber experiments with CS1-CS5. In addition to the minute-by-minute data, binned values as a function of attenuation were generated using the Python function 'np.histogram_bin_edges' and the 'fd' method. Figure S5.a reveals that even after the internal correction applied in real-time by the aethalometer, a dependency of the C factor on attenuation remains evident. Specifically, the correction tends to be overestimated by up to 20% following a filter change when attenuation values are below 10. Conversely, C is underestimated by up to 20% before the next filter change, particularly at attenuation values exceeding 50. This residual dependency introduces a notable bias in the average C values, especially in scenarios where the absorption Ångstrom exponent is high, and filter changes occur at ATN values (660 nm) close to 10.

We examined the dependence of C on attenuation using data corrected for the loading effect through the other methods described in Sect. 2.2.1: W2003, C2010, Dual Spot and the fitting method. Results for these different correction algorithms are also shown in Fig. S4. The C2010 method (Figure S5.b) introduces a significant bias, with a spread of up to 45% for C, particularly below an ATN of 20. The W2003 method (Figure S5.c) reduces this bias to approximately 35%, but still leaves notable inaccuracies, especially at low attenuation values (<10). The Dual Spot method (Figure S5.d) reduce the bias but introducing inaccuracies for high attenuation (>50), without solving the jumps between spots (Figure S4). Based on these findings, we applied the fitting method to all data for subsequent analyses. This approach minimizes potential biases when comparing average C values across different experiments and filter spots. However, it is important to note that this method may not be suitable for conditions with greater variability in particle properties, where the assumption of a constant C value over time may not hold.

S3. Cross-sensitivity of the C-size dependence on the loading correction scheme

Analysis of the cross-sensitivity of the C-size dependence on the loading correction scheme applied suggests that the C increase for decreasing sizes is evident regardless of the correction method used (Figure S6). The largest increase (88%) occurs with the C2010 method, while the smallest (44%) is seen with the W2003 method. The internal correction and Dual Spot methods both yield a 71% increase, similar to the 77% obtained with the fitting method developed in this study. However, for the internal correction method, the C increase is observed to start at larger diameters, extending to CS1–CS4 particles. In consequence, with the internal correction, differences of C between CS types at similar sizes become negligible, suggesting that size remains the dominant factor.

S4. Identification of dust transport days

Dust transport days were identified following the method described in detail in Duchi et al. (2016), which combines in-situ measurements of the coarse particle concentration (particles with a diameter larger than 1 µm) and backward trajectories. The coarse particle concentration is obtained from measurements of an optical particle counter (Grimm® model 1.108). The data are averaged over 24h. On the time series of daily data, a multi-step smoothing is applied, and subtracted from the original time series to obtain the high frequency component. If a data point of the high frequency component exceeds the threshold value given as the 95^{th} confidence interval, it is flagged as a potential dust transport day. For these potential dust transport days 7-day backward trajectories are take and if they passed over the Saharan desert, the according days is finally flagged as a dust transport day.

The particulate matter concentration of the coarse particles (PMcoarse) is calculated from the coarse particle size distribution measured by the optical particle counter and a particle size dependent density (Wittmaack, 2002).

References

Cuesta-Mosquera, A., Močnik, G., Drinovec, L., Müller, T., Pfeifer, S., Minguillón, M. C., Briel, B., Buckley, P., Dudoitis, V., Fernández-García, J., Fernández-Amado, M., Ferreira De Brito, J., Riffault, V., Flentje, H., Heffernan, E., Kalivitis, N., Kalogridis, A.-C., Keernik, H., Marmureanu, L., Luoma, K., Marinoni, A., Pikridas, M., Schauer, G., Serfozo, N., Servomaa, H., Titos, G., Yus-Díez, J., Zioła, N., and Wiedensohler, A.: Intercomparison and characterization of 23 Aethalometers under laboratory and ambient air conditions: procedures and unit-to-unit variabilities, Atmospheric Measurement Techniques, 14, 3195–3216, https://doi.org/10.5194/amt-14-3195-2021, 2021.

Drinovec, L., Močnik, G., Zotter, P., Prévôt, A. S. H., Ruckstuhl, C., Coz, E., Rupakheti, M., Sciare, J., Müller, T., Wiedensohler, A., and Hansen, A. D. A.: The "dual-spot" Aethalometer: an improved measurement of aerosol black carbon with real-time loading compensation, Atmospheric Measurement Techniques, 8, 1965–1979, https://doi.org/10.5194/amt-8-1965-2015, 2015.

Duchi, R., Cristofanelli, P., Landi, T. C., Arduini, J., Bonafe', U., Bourcier, L., Busetto, M., Calzolari, F., Marinoni, A., Putero, D., and Bonasoni, P.: Long-term (2002–2012) investigation of Saharan dust transport events at Mt. Cimone GAW global station, Italy (2165 m a.s.l.), Elementa: Science of the Anthropocene, journalAbbreviation: Elem Sci Anth, 000085, https://doi.org/10.12952/journal.elementa.000085, 2016.

Heuser, J., Di Biagio, C., Yon, J., Cazaunau, M., Bergé, A., Pangui, E., Zanatta, M., Renzi, L., Marinoni, A., Inomata, S., Yu, C., Bernardoni, V., Chevaillier, S., Ferry, D., Laj, P., Maillé, M., Massabò, D., Mazzei, F., Noyalet, G., Tanimoto, H., Temime-Roussel, B., Vecchi, R., Vernocchi, V., Formenti, P., Picquet-Varrault, B., and Doussin, J.-F.: Spectral optical properties of soot: laboratory investigation of propane flame particles and their link to composition, Atmospheric Chemistry and Physics, 25, 6407–6428, https://doi.org/10.5194/acp-25-6407-2025, 2025.

Wittmaack, K.: Advanced evaluation of size-differential distributions of aerosol particles, Journal of Aerosol Science, 33, 1009–1025, 2002.